

Genetic design of solids possessing a random–particulate microstructure

T. I. Zohdi

Phil. Trans. R. Soc. Lond. A 2003 **361**, 1021–1043

doi: 10.1098/rsta.2003.1179

Rapid response

[Respond to this article](#)

<http://rsta.royalsocietypublishing.org/letters/submit/roypta;361/1806/1021>

Email alerting service

Receive free email alerts when new articles cite this article - sign up in the box at the top right-hand corner of the article or click [here](#)

To subscribe to *Phil. Trans. R. Soc. Lond. A* go to: <http://rsta.royalsocietypublishing.org/subscriptions>

Genetic design of solids possessing a random-particulate microstructure

BY T. I. ZOHDI

*Department of Mechanical Engineering, 6195 Etcheverry Hall,
University of California, Berkeley, CA 94720-1740, USA*

Published online 26 March 2003

There exists a variety of difficulties in the computational design of macroscopic solid material properties formed by doping a homogeneous base matrix material with randomly distributed particles having different properties. Three primary problems are

- (1) the wide array of free microdesign variables, such as particle topology, property phase contrasts and volume fraction, which render the associated objective functions to be highly non-convex;
- (2) that the associated objective functions are not differentiable with respect to design variables, primarily due to prescribed constraints, such as prespecified restrictions on the microscale stress-field behaviour; and
- (3) the effective responses of various finite-sized samples, of equal volume but of different random particle distributions, exhibit mutual fluctuations, leading to amplified noise in optimization strategies where objective function sensitivities or comparisons are needed.

The focus of this paper is the development of a statistical genetic algorithm which can handle difficulties due to non-convexity, lack of regularity and size effects. Theoretical properties of the overall approach are investigated. Semi-analytical and large-scale numerical examples, involving finite-element type discretizations, are given to illustrate its practical application.

Keywords: genetic algorithms; random particulates; inverse problems

1. Basic concepts in macro-micromodelling

A growing variety of new solid materials possessing random heterogeneous microstructure is used in modern applications. An extensive review of the state of the art in the analysis of random heterogeneous media can be found in Torquato (1991, 1997, 1998, 2002). One class of such materials consists of particles or fibres suspended in a binding matrix material. The mechanical properties of microheterogeneous materials are characterized by a spatially variable elasticity tensor \mathbb{E} , while the (homogenized) effective macroscopic response is described via $\langle \boldsymbol{\sigma} \rangle_{\Omega} = \mathbb{E}^* : \langle \boldsymbol{\epsilon} \rangle_{\Omega}$, where

$$\langle \cdot \rangle_{\Omega} \stackrel{\text{def}}{=} \frac{1}{|\Omega|} \int_{\Omega} \cdot \, d\Omega,$$

One contribution of 12 to a Theme ‘Micromechanics of fluid suspensions and solid composites’.

and where $\boldsymbol{\sigma}$ and $\boldsymbol{\epsilon}$ are the stress and strain tensor fields within a statistically representative volume element (RVE) of volume $|\Omega|$. The quantity \mathbb{E}^* , known as the effective property, is the elasticity tensor used in usual structural scale analyses. Similarly, one can describe other effective quantities, such as conductivity or diffusivity, relating other volumetrically averaged field variables. *It is emphasized that effective quantities such as \mathbb{E}^* are not material properties, but relations between averages.* More appropriate terms might be ‘apparent properties’, which are discussed in depth in Huet (1990). However, to be consistent with the literature, we continue to refer to \mathbb{E}^* by the somewhat inaccurate term effective ‘property’.

Ideally, one would like to evaluate a new material’s behaviour by numerical simulations, with the primary goal being to accelerate expensive trial and error laboratory tests. However, there exist a variety of difficulties in the computational design of macroscopic solid material properties formed by doping a base matrix material with randomly distributed particles of different phases. Three primary problems are

- (1) the wide array of free microdesign variables, such as particle topology, volume fraction and mechanical property phase contrasts, which render associated objective functions to be highly non-convex;
- (2) that the associated objective functions are not continuously differentiable with respect to design space, primarily due to microscale design constraints, such as restrictions on microscale stress-field behaviour; and
- (3) the effective responses of various finite-sized samples, of equal volume but of different random distributions of the particulate matter, exhibit mutual fluctuations, leading to amplified noise in optimization strategies where objective function sensitivities or comparisons are needed.

The effects in problem 3 become even more critical when computing design sensitivities or comparisons needed in optimization strategies.

The presented work concentrates on the parametrization of microscale parameters inherent in such materials, with the goal of computational optimization of material microstructure. The outline of the presentation is as follows. A computational material design (inverse) formulation is given. Attention is drawn to some of the difficulties encountered, i.e. non-convexity and non-differentiability of objective functions, as well as size effects. A statistical genetic algorithm, which can handle difficulties due to non-convexity, lack of regularity and size effects is then developed. Numerical examples are then presented.

2. Computational material design

We are primarily concerned with the construction of an inverse problem, where combinations of particulate and matrix materials are sought which minimize the following normalized objective function

$$\Pi = \left(\frac{\|\mathbb{E}^* - \mathbb{E}^{*,D}\|}{\|\mathbb{E}^{*,D}\|} \right)^p, \quad (2.1)$$

where $\mathbb{E}^{*,D}$ is a prespecified desired effective response, \mathbb{E}^* is the effective response produced by a trial microstructure, and $\|\cdot\|$ is an appropriate admissible norm to be

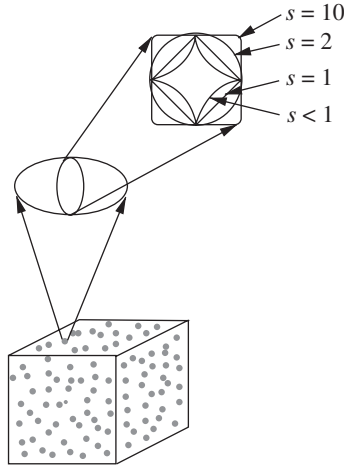


Figure 1. Parametrization of a generalized ellipsoid, with various parametrized cross-sections shown.

discussed later. A microstructural design can be defined through an N -tuple design vector, denoted $\mathbf{A} \stackrel{\text{def}}{=} (A_1, A_2, \dots, A_N)$, consisting of the following components, for example: the mechanical properties of the foreign particulate matter; the volume fraction of the foreign particulate matter; and the topology of the foreign particulate matter. Ellipsoidal shapes are qualitatively useful, since the geometry can closely represent a variety of particulate types, for example, platelets when the ellipsoids are oblate or needles (discontinuous fibres) when the ellipsoids are prolate. Such shapes can be generalized by considering (figure 1)

$$\left(\frac{|x-x_0|}{r_1}\right)^{s_1} + \left(\frac{|y-y_0|}{r_2}\right)^{s_2} + \left(\frac{|z-z_0|}{r_3}\right)^{s_3} = 1, \quad (2.2)$$

where the s are exponents. Values of $s < 1$ produce non-convex shapes, while $s > 2$ values produce ‘blocklike’ shapes. The following are free variables.

Particulate mechanical properties: for example, assuming local isotropy of the particles, the bulk and shear moduli, κ_2 and μ_2 (two variables).

Particulate topology: for example, the polynomial order of generalized ellipsoids, s (three variables).

Particulate aspect ratio: for example, defined by $A \stackrel{\text{def}}{=} r_1/r_2 = r_1/r_3$, where $r_2 = r_3$, $A > 1$ for prolate geometries and $A < 1$ for oblate shapes (one variable).

Particulate volume fraction: for example, $v_2 \stackrel{\text{def}}{=} |\Delta|/|\Omega|$, where $|\Delta|$ is the volume occupied by the particles, and $|\Omega|$ is the total volume of the material (one variable).

Particulate orientation: for example, within the last decade there have viable been processing methods developed to control the orientation of particulate matter by coating them with a conducting liquid material and introducing them into the molten matrix material (three free variables, i.e. Euler angles). Thereafter, an

electrical current is applied, forcing the particles to align themselves along the field lines. This can produce globally anisotropic properties (see Michaud (1992) for manufacturing details of this and alternative processes).

Matrix mechanical properties: for example, if the matrix material is variable, assuming local isotropy of the matrix material, κ_1 and μ_1 (two variables).

Therefore, in this linear elasticity formulation, we have 12 microdesign variables. We remark that for both manufacturing and physical reasons, generally, each design variable will have a constrained search space. For example, none of the design variables in this formulation can be negative, with the exception of the orientation angles; furthermore, the volume fraction must be less than one. Further discussions of inverse formulations of this kind can be found in Hyun & Torquato (2001) and Torquato & Hyun (2001).

3. Mathematical setting

In order to drive material design algorithms, an effective property \mathbb{E}^* for each trial microstructural design vector must be generated. This computation requires a somewhat precise mathematical statement. Consider a sample of heterogeneous material occupying an open bounded domain in $\Omega \in \mathbb{R}^3$, under a given set of specified boundary loadings. Its boundary is denoted $\partial\Omega$. The body is in static equilibrium under the action of body forces, \mathbf{f} , and surface tractions, \mathbf{t} . The boundary $\partial\Omega = \Gamma_u \cup \Gamma_t$ consists of a part Γ_u and a part Γ_t on which displacements and tractions are respectively prescribed. Following standard notation, $H^1(\Omega)$ is denoted as the usual space of functions with generalized partial derivatives of order one or less in $L^2(\Omega)$. The symbol

$$\mathbf{H}^1(\Omega) \stackrel{\text{def}}{=} [H^1(\Omega)]^3$$

is defined as the space of vector-valued functions whose components have generalized partial derivatives up to one in $\mathbf{L}^2(\Omega) \stackrel{\text{def}}{=} [L^2(\Omega)]^3$. The symbol ' $\mathbf{u}|_{\partial\Omega}$ ' is used for generalized boundary values, for example, for specified boundary displacements. Throughout the analysis, the microstructure is assumed to be perfectly bonded. A general variational boundary-value representation is given by finding $\mathbf{u} \in \mathbf{H}^1(\Omega)$, $\mathbf{u}|_{\Gamma_u} = \mathbf{d}$, such that

$$\int_{\Omega} \nabla \mathbf{v} : \mathbb{E} : \nabla \mathbf{u} \, d\Omega = \int_{\Omega} \mathbf{f} \cdot \mathbf{v} \, d\Omega + \int_{\Gamma_t} \mathbf{t} \cdot \mathbf{v} \, dA, \quad \forall \mathbf{v} \in \mathbf{H}^1(\Omega), \quad \mathbf{v}|_{\Gamma_u} = \mathbf{0}. \quad (3.1)$$

The data are assumed to be such that $\mathbf{f} \in \mathbf{L}^2(\Omega)$ and $\mathbf{t} \in \mathbf{L}^2(\Gamma_t)$, but less smooth data can be considered without complications. It is convenient to consider the sample domain (Ω) as a cube, although, strictly speaking, this is not necessary. A commonly accepted macro/micro criterion used in effective property calculations is the well-known Hill (1952) condition $\langle \boldsymbol{\sigma} : \boldsymbol{\epsilon} \rangle_{\Omega} = \langle \boldsymbol{\sigma} \rangle_{\Omega} : \langle \boldsymbol{\epsilon} \rangle_{\Omega}$. Hill's condition dictates the size requirements on the sample for it to be statistically representative. The classical argument is as follows. For any perfectly bonded heterogeneous body, in the absence of body forces ($\mathbf{f} = \mathbf{0}$), two physically relevant loading states satisfy Hill's condition. They are (i) purely linear boundary displacements of the form $\mathbf{u}|_{\partial\Omega} = \boldsymbol{\mathcal{E}} \cdot \mathbf{x}$, which implies $\langle \boldsymbol{\epsilon} \rangle_{\Omega} = \boldsymbol{\mathcal{E}}$, and (ii) pure boundary tractions in the form $\mathbf{t}|_{\partial\Omega} = \boldsymbol{\mathcal{L}} \cdot \mathbf{n}$, which implies $\langle \boldsymbol{\sigma} \rangle_{\Omega} = \boldsymbol{\mathcal{L}}$, where $\boldsymbol{\mathcal{E}}$ and $\boldsymbol{\mathcal{L}}$ are constant strain and stress tensors, respectively. Clearly, for Hill's condition to be satisfied within a macroscopic body under non-uniform external loading, the sample must be large enough to possess

small boundary field fluctuations relative to its size. Therefore, applying type (i) or (ii) boundary conditions to a large sample is a way of reproducing approximately what may be occurring in a statistically representative mesoscopic subdomain of material within a macroscopic body. Usually, in order to justify the interchangeable use of either boundary loading, the sample must be large with respect to the inhomogeneities. Explicitly, to determine \mathbb{E}^* , one specifies six linearly independent loadings of the form (i) $\mathbf{u}|_{\partial\Omega} = \mathcal{E}^{(I \rightarrow VI)} \cdot \mathbf{x}$ or (ii) $\mathbf{t}|_{\partial\Omega} = \mathcal{L}^{(I \rightarrow VI)} \cdot \mathbf{n}$, where $\mathcal{E}^{(I \rightarrow VI)}$ and $\mathcal{L}^{(I \rightarrow VI)}$ are symmetric second-order strain and stress tensors, with spatially constant components. Each independent loading state provides six equations, for a total of 36, which are used to determine the tensor relation between average stress and strain, \mathbb{E}^* . If the effective response is assumed to be isotropic, then only one test loading (instead of usually six), possessing non-zero dilatational ($\frac{1}{3} \text{tr } \boldsymbol{\sigma}$ and $\frac{1}{3} \text{tr } \boldsymbol{\epsilon}$) and deviatoric components ($\boldsymbol{\sigma}'$ and $\boldsymbol{\epsilon}'$), is necessary to determine the effective bulk and shear moduli, which can be defined by

$$3\kappa^* \stackrel{\text{def}}{=} \frac{\langle \frac{1}{3} \text{tr } \boldsymbol{\sigma} \rangle_{\Omega}}{\langle \frac{1}{3} \text{tr } \boldsymbol{\epsilon} \rangle_{\Omega}} \quad \text{and} \quad 2\mu^* \stackrel{\text{def}}{=} \sqrt{\frac{\langle \boldsymbol{\sigma}' \rangle_{\Omega} : \langle \boldsymbol{\sigma}' \rangle_{\Omega}}{\langle \boldsymbol{\epsilon}' \rangle_{\Omega} : \langle \boldsymbol{\epsilon}' \rangle_{\Omega}}}.$$

Remark 3.1. Difficulties arise whenever one attempts to design the effective mechanical properties of particulate materials, which on a practical level involves finite-sized samples possessing an irregular heterogeneous microstructure. These difficulties are discussed next.

4. Minimization methods

Following a standard Newton-type multivariate search, a new design increment, $\Delta = (\Delta\Lambda_1, \Delta\Lambda_2, \dots, \Delta\Lambda_N)$ for a microstructural design vector Λ , is achieved by solving the system $[H]\{\Delta\Lambda\} = -\{\mathbf{g}\}$, where $[H]$ is the Hessian matrix ($N \times N$), with components

$$H_{ij} = \frac{\partial^2 \Pi(\Lambda)}{\partial \Lambda_i \partial \Lambda_j},$$

$\{\mathbf{g}\}$ is the gradient ($N \times 1$), with components $g_i = \partial \Pi(\Lambda) / \partial \Lambda_i$ and where $\{\Delta\Lambda\}$ is the design increment ($N \times 1$), with components $\Delta\Lambda_i$. After the design increment has been solved for, one then forms an updated design vector, $\Lambda^{\text{new}} = \Lambda^{\text{old}} + \Delta\Lambda$, and the process is repeated until $\|\Pi\| \leq \text{tol}$. Explicitly, the incremental system is

$$\begin{bmatrix} \frac{\partial^2 \Pi(\Lambda)}{\partial \Lambda_1 \partial \Lambda_1} & \frac{\partial^2 \Pi(\Lambda)}{\partial \Lambda_1 \partial \Lambda_2} & \frac{\partial^2 \Pi(\Lambda)}{\partial \Lambda_1 \partial \Lambda_3} & \frac{\partial^2 \Pi(\Lambda)}{\partial \Lambda_1 \partial \Lambda_4} & \cdots \\ \frac{\partial^2 \Pi(\Lambda)}{\partial \Lambda_2 \partial \Lambda_1} & \frac{\partial^2 \Pi(\Lambda)}{\partial \Lambda_2 \partial \Lambda_2} & \frac{\partial^2 \Pi(\Lambda)}{\partial \Lambda_2 \partial \Lambda_3} & \frac{\partial^2 \Pi(\Lambda)}{\partial \Lambda_2 \partial \Lambda_4} & \cdots \\ \frac{\partial^2 \Pi(\Lambda)}{\partial \Lambda_3 \partial \Lambda_1} & \frac{\partial^2 \Pi(\Lambda)}{\partial \Lambda_3 \partial \Lambda_2} & \frac{\partial^2 \Pi(\Lambda)}{\partial \Lambda_3 \partial \Lambda_3} & \frac{\partial^2 \Pi(\Lambda)}{\partial \Lambda_3 \partial \Lambda_4} & \cdots \\ \frac{\partial^2 \Pi(\Lambda)}{\partial \Lambda_4 \partial \Lambda_1} & \frac{\partial^2 \Pi(\Lambda)}{\partial \Lambda_4 \partial \Lambda_2} & \frac{\partial^2 \Pi(\Lambda)}{\partial \Lambda_4 \partial \Lambda_3} & \frac{\partial^2 \Pi(\Lambda)}{\partial \Lambda_4 \partial \Lambda_4} & \cdots \\ \vdots & \vdots & \vdots & \vdots & \ddots \\ \frac{\partial^2 \Pi(\Lambda)}{\partial \Lambda_N \partial \Lambda_1} & \frac{\partial^2 \Pi(\Lambda)}{\partial \Lambda_N \partial \Lambda_2} & \frac{\partial^2 \Pi(\Lambda)}{\partial \Lambda_N \partial \Lambda_3} & \frac{\partial^2 \Pi(\Lambda)}{\partial \Lambda_N \partial \Lambda_4} & \cdots \end{bmatrix} \begin{Bmatrix} \Delta\Lambda_1 \\ \Delta\Lambda_2 \\ \Delta\Lambda_3 \\ \Delta\Lambda_4 \\ \vdots \\ \Delta\Lambda_N \end{Bmatrix} = - \begin{Bmatrix} \frac{\partial \Pi(\Lambda)}{\partial \Lambda_1} \\ \frac{\partial \Pi(\Lambda)}{\partial \Lambda_2} \\ \frac{\partial \Pi(\Lambda)}{\partial \Lambda_3} \\ \frac{\partial \Pi(\Lambda)}{\partial \Lambda_4} \\ \vdots \\ \frac{\partial \Pi(\Lambda)}{\partial \Lambda_N} \end{Bmatrix}. \quad (4.1)$$

(a) *Difficulties due non-convexity*

A severe difficulty is that the system in equation (4.1) becomes non-invertible throughout the design space, due to the non-convexity of the objective function Π . We illustrate the problem of non-convexity via a simple one-dimensional example. Consider a simple one-dimensional bar of length L composed of random particles, i.e. strips in one dimension. There are a total of N strips: N_2 dark strips, each of thickness a , and N_1 white strips representing the rest of the material. Young's modulus E_2 corresponds to the 'particles', while E_1 corresponds the 'matrix'. Suppose one wishes to design an effective response, E^* , of such a structure, defined by $\langle \sigma \rangle_\Omega = E^* \langle \epsilon \rangle_\Omega$. Consider the two-point boundary-value problem

$$\frac{d}{dx} \left(E \frac{du}{dx} \right) = 0, \quad u(0) = 0, \quad u(L) = \mathcal{E} \times L,$$

where \mathcal{E} is a constant. One finds that the effective response is the harmonic average, which can be written as

$$E^* = \frac{\tau E_1}{(1 - v_2)\tau + v_2}, \quad (4.2)$$

where $\tau = E_2/E_1$, $v_1 + v_2 = 1$ and $v_2 = N_2 a/L$. Clearly, there is no unique combination of τ and v_2 to produce the same desired effective response. Consider

$$\Pi = \left(\frac{E^* - E^{*,D}}{E^{*,D}} \right)^2, \quad (4.3)$$

where $E^{*,D}$ is a desired effective response. Following a standard Newton-type multivariate search (a new design increment), one would obtain the following Hessian system for the two design variables $\tau = E_2/E_1$ and v_2 :

$$\begin{bmatrix} \frac{\partial^2 \Pi(\tau, v_2)}{\partial \tau^2} & \frac{\partial^2 \Pi(\tau, v_2)}{\partial \tau \partial v_2} \\ \frac{\partial^2 \Pi(\tau, v_2)}{\partial v_2 \partial \tau} & \frac{\partial^2 \Pi(\tau, v_2)}{\partial v_2^2} \end{bmatrix} \begin{Bmatrix} \Delta \tau \\ \Delta v_2 \end{Bmatrix} = - \begin{Bmatrix} \frac{\partial \Pi(\tau, v_2)}{\partial \tau} \\ \frac{\partial \Pi(\tau, v_2)}{\partial v_2} \end{Bmatrix}. \quad (4.4)$$

However, this system becomes non-invertible throughout the design space, due to the non-convexity of the objective function Π . For an example see figure 2. For more details on non-uniqueness of solutions and non-convexity of the associated objective functions, see Cherkav (2000).

(b) *Local field design constraints*

Consider the deviation of the stress field from its volumetric average, $\delta \sigma = \sigma - \langle \sigma \rangle_\Omega$, which leads to

$$\langle \sigma : \sigma \rangle_\Omega = \frac{1}{|\Omega|} \int_\Omega \sigma : \sigma \, d\Omega = \langle \sigma \rangle_\Omega : \langle \sigma \rangle_\Omega + \frac{1}{|\Omega|} \int_\Omega \delta \sigma : \delta \sigma \, d\Omega \geq 0. \quad (4.5)$$

Therefore

$$\frac{\langle \sigma : \sigma \rangle_\Omega - \langle \sigma \rangle_\Omega : \langle \sigma \rangle_\Omega}{\langle \sigma : \sigma \rangle_\Omega} = \frac{\langle \delta \sigma : \delta \sigma \rangle_\Omega}{\langle \sigma : \sigma \rangle_\Omega} \geq 0. \quad (4.6)$$

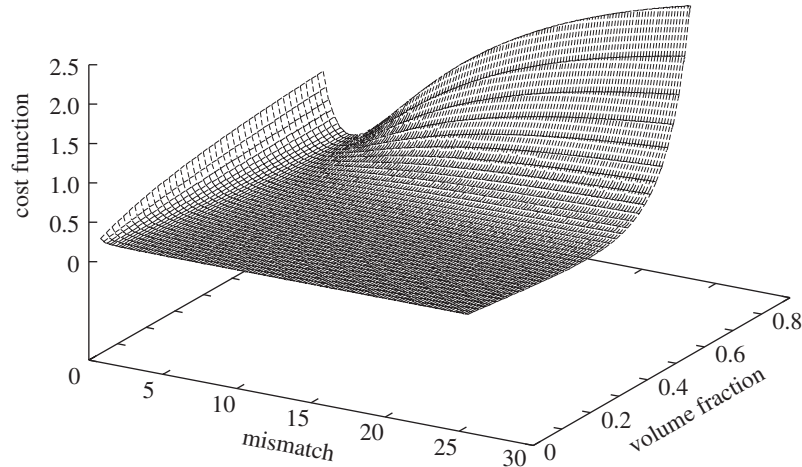


Figure 2. The behaviour of the objective function for $E_1 = 1$ and $E^{*,D} = 1.75$.

In order to incorporate the deviation in a cost function, we introduce a tolerance, tol_σ , where, ideally,

$$\sqrt{\frac{\langle \delta \boldsymbol{\sigma} : \delta \boldsymbol{\sigma} \rangle_\Omega}{\langle \boldsymbol{\sigma} : \boldsymbol{\sigma} \rangle_\Omega}} \leq \text{tol}_\sigma. \quad (4.7)$$

If the normalized deviation exceeds tol_σ , then the level of exceedance is incorporated as a multilateral constraint to the macroscopic objectives by

$$\Pi = \underbrace{\left(\frac{\|\mathbb{E}^* - \mathbb{E}^{*,D}\|}{\|\mathbb{E}^{*,D}\|} \right)^p}_{\text{macro-objective}} + w_\sigma \underbrace{\left(\frac{\sqrt{\langle \delta \boldsymbol{\sigma} : \delta \boldsymbol{\sigma} \rangle_\Omega / \langle \boldsymbol{\sigma} : \boldsymbol{\sigma} \rangle_\Omega}}{\text{tol}_\sigma} - 1 \right)^q}_{\text{microfield smoothness}}, \quad (4.8)$$

where p and q are non-negative and where $w_\sigma = 0$ if

$$\frac{\langle \delta \boldsymbol{\sigma} : \delta \boldsymbol{\sigma} \rangle_\Omega}{\langle \boldsymbol{\sigma} : \boldsymbol{\sigma} \rangle_\Omega} \leq \text{tol}_\sigma$$

and $w_\sigma > 0$ otherwise. Detailed examples will be given shortly.

(c) Difficulties due to non-differentiability

Due to the presence of design constraints, the objective may be non-differentiable independent of the problem with non-convexity. For most complicated systems, usually finite-difference approximations of the gradient and Hessian components are constructed with respect to the design parameters. The finite-difference size for the approximate numerical derivatives, which is different for each component, is denoted h_{A_i} . In a practical setting, for example, for each variable, the numerical derivative step sizes are scaled to the size of the current value of that variable, by a small number $0 < \theta \ll 1$, $\theta \times A_i = h_{A_i}$. Numerically, the components of the gradient and Hessian can be approximated by the following second-order central finite-difference

stencils such as

$$\begin{aligned} \frac{\partial^2 \Pi(\mathbf{\Lambda})}{\partial \Lambda_i \partial \Lambda_j} \approx & \frac{\Pi(\Lambda_1, \Lambda_2 \dots \Lambda_i + h_{\Lambda_i}, \dots \Lambda_j + h_{\Lambda_j}, \dots \Lambda_N)}{4h_{\Lambda_i} h_{\Lambda_j}} \\ & + \frac{\Pi(\Lambda_1, \Lambda_2 \dots \Lambda_i - h_{\Lambda_i}, \dots \Lambda_j - h_{\Lambda_j}, \dots \Lambda_N)}{4h_{\Lambda_i} h_{\Lambda_j}} \\ & - \frac{\Pi(\Lambda_1, \Lambda_2 \dots \Lambda_i - h_{\Lambda_i}, \dots \Lambda_j + h_{\Lambda_j}, \dots \Lambda_N)}{4h_{\Lambda_i} h_{\Lambda_j}} \\ & + \frac{\Pi(\Lambda_1, \Lambda_2 \dots \Lambda_i + h_{\Lambda_i}, \dots \Lambda_j - h_{\Lambda_j}, \dots \Lambda_N)}{4h_{\Lambda_i} h_{\Lambda_j}}. \end{aligned} \quad (4.9)$$

The number of objective function evaluations necessary to form the Hessian and gradient is $2N^2 + 1$, where N is the number of microstructural design variables. This stems from the fact that one needs $2(N^2 - N)$ objective evaluations for the off-diagonal terms of the Hessian, $2N$ for the diagonal terms, and one evaluation for the base point (the current design). Therefore, even with a small number of design variables the number of objective function evaluations can be quite large. For example, with the 12 microstructural variables introduced earlier, $N = 12$, and one has $2N^2 + 1 = 2(12)^2 + 1 = 289$ objective function evaluations per search step. It is clear that the construction of the discrete Hessian is the main expense. There exist a variety of quasi-Newton methods, which in some manner attempt to approximate the Hessian in an inexpensive way (see Gill *et al.* 1995). However, regardless of the reduction in the number costly objective function evaluations, such procedures require an immense amount of effort, which grows dramatically with sample size. Implicitly, such objective functions require a sufficient degree of regularity for the derivatives to make sense. For example, due to the fact that design constraints are present, there are many points throughout the domain where the objective function is not twice differentiable, implying

$$\frac{\partial^2 \Pi(\Lambda)}{\partial \Lambda_i \partial \Lambda_j} \neq \frac{\partial^2 \Pi(\Lambda)}{\partial \Lambda_j \partial \Lambda_i},$$

thus rendering the Hessian matrix non-symmetric. This implies that the second-order finite-difference stencils are insufficient, since they inherently construct a symmetric approximation to the Hessian. Therefore, their use to construct the numerical Hessian can only be justified near smooth convex optima. To put it succinctly, such methods are not robust. For an investigation of the performance of gradient methods for the design of materials possessing random microstructure we refer the reader to Zohdi (2001, 2002a).

5. Non-convex–non-derivative genetic search

The lack of *robustness* of classical gradient based deterministic optimization processes can be rectified by application of a family of methods, usually termed ‘genetic’ algorithms. Genetic algorithms are search methods based on the principles of natural selection and, as such, they are highly probabilistic. There is a variety of such methods, which employ concepts of species evolution, such as reproduction, mutation and

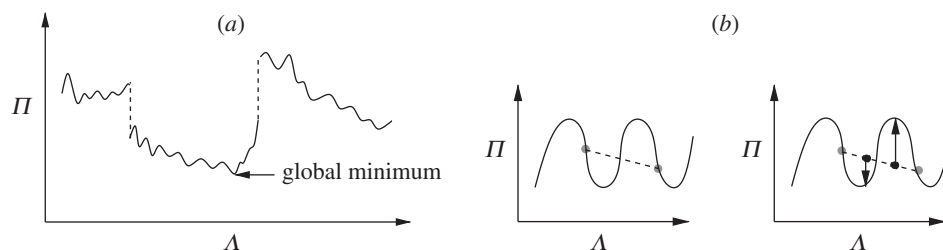


Figure 3. (a) A characterization of the class of objective functions of interest. (b) A loss of superior older genetic strings if the top parents are not retained.

crossover. Such methods stem from the work of John Holland and his colleagues in the late 1960s and early 1970s at the University of Michigan (Holland 1975). For reviews of such methods, the interested reader is referred to Goldberg (1989), Davis (1991) and Onwubiko (2000). A recent overview of the state of the art of the field can be found in a collection of recent articles, edited by Goldberg & Deb (2000). In Zohdi (2002*b*) a genetic algorithm was developed by combining the basic ideas used in the Genetic algorithm community. Specifically, genetic-type algorithms were developed for non-convex inverse problems of micro-macromaterials design for non-stochastic problems without constraints. Presently, we build upon this algorithm further and apply it to the more complicated random systems, with constraints, of interest here. The key conceptual feature is that the microstructural parameters form a ‘genetic string’. Thereafter, evolutionary concepts are applied to a population of such strings. The algorithm is straightforward and is as follows:

- Step 1 randomly select n starting genetic strings \mathbf{A}^i ($i = 1, \dots, N$):
 $\mathbf{A}^i \stackrel{\text{def}}{=} \{A_1^i, A_2^i, A_3^i, A_4^i, A_5^i \dots\}$
 (for example: $\mathbf{A}^i \stackrel{\text{def}}{=} \{\kappa_2^i, \mu_2^i, v_2^i, A^i, s^i \dots\}$)
- Step 2 compute fitness ($\Pi(\mathbf{A}^i)$) of each genetic string: ($i = 1, \dots, N$)
- Step 3 rank the genetic strings, \mathbf{A}^i ($i = 1, \dots, N$)
- Step 4 mate nearest pairs (produce offspring) ($i = 1, \dots, N$)
 $\boldsymbol{\lambda}^i \stackrel{\text{def}}{=} \Phi^{(I)}\mathbf{A}^i + (1 - \Phi^{(I)})\mathbf{A}^{i+1}$, $\boldsymbol{\lambda}^{i+1} \stackrel{\text{def}}{=} \Phi^{(II)}\mathbf{A}^i + (1 - \Phi^{(II)})\mathbf{A}^{i+1}$,
 $0 \leq \Phi^{(I)}, \Phi^{(II)} = \text{RAND} \leq 1$ (different for each component)
- Step 5 enforce design constraints: $\kappa_2^{(-)} \leq \kappa_2^i \leq \kappa_2^{(+)}$, $\mu_2^{(-)} \leq \mu_2^i \leq \mu_2^{(+)}$, ...
- Step 6 kill off bottom $m < n$ strings. Optional: keep top k parents
- Step 7 repeat with top gene pool plus m new genetic strings.

We remark that the definition of ‘fitness’ of a genetic string in this algorithm indicates the value of the objective function. In other words, the most fit genetic string is simply the one with the smallest objective function. Steps 1–7, which are associated with the genetic part of the overall algorithm, attempt to collect multiple local minima.† At first glance, it seems somewhat superfluous to retain even the top

† It is remarked that if the function Φ is allowed to be greater than unity one can consider the resulting convex combination (offspring) as a ‘mutation’.

parents in such an algorithm. However, as we will illustrate shortly, by implementing the algorithm above, it is found that retention of the best old genetic strings is critical. From figure 3 one sees that, if the objective functions are highly non-convex, there exists a strong possibility that the inferior offspring will replace superior parents. Therefore, retaining the top parents is not only less computationally expensive, since these designs do not have to be re-evaluated, it is theoretically superior. With parent retention, the minimization of the cost function is guaranteed to be monotonic with increasing generations.

(a) *A deterministic example*

As an example, consider the widely used Hashin & Shtrikman (1962, 1963) bounds for isotropic materials with isotropic effective responses; for the bulk moduli,

$$\begin{aligned} \kappa^{*, -} &\stackrel{\text{def}}{=} \kappa_1 + v_2 \left(\frac{1}{\kappa_2 - \kappa_1} + \frac{3(1 - v_2)}{3\kappa_1 + 4\mu_1} \right)^{-1} \\ &\leq \kappa^* \leq \kappa_2 + (1 - v_2) \left(\frac{1}{\kappa_1 - \kappa_2} + \frac{3v_2}{3\kappa_2 + 4\mu_2} \right)^{-1} \stackrel{\text{def}}{=} \kappa^{*, +}, \end{aligned} \quad (5.1)$$

and for the shear moduli

$$\begin{aligned} \mu^{*, -} &\stackrel{\text{def}}{=} \mu_1 + v_2 \left(\frac{1}{\mu_2 - \mu_1} + \frac{6(1 - v_2)(\kappa_1 + 2\mu_1)}{5\mu_1(3\kappa_1 + 4\mu_1)} \right)^{-1} \\ &\leq \mu^* \leq \mu_2 + (1 - v_2) \left(\frac{1}{\mu_1 - \mu_2} + \frac{6v_2(\kappa_2 + 2\mu_2)}{5\mu_2(3\kappa_2 + 4\mu_2)} \right)^{-1} \stackrel{\text{def}}{=} \mu^{*, +}, \end{aligned} \quad (5.2)$$

where κ_2 and κ_1 are the bulk moduli and μ_2 and μ_1 are the shear moduli of the respective phases ($\kappa_2 \geq \kappa_1$) and ($\mu_2 \geq \mu_1$), and where v_2 is the second phase volume fraction. Such bounds are the tightest known on isotropic effective responses, with isotropic two-phase microstructures, where only the volume fractions and phase contrasts of the constituents are known. As we have mentioned earlier, during effective material design development, when selecting particulate micro-additives for a base matrix, information about the changes in the otherwise (relatively) smooth internal fields, corresponding to the matrix material alone, is valuable to characterize a new tailored material's performance. For the purposes of this example, one way to analytically characterize the smoothness of the microscopic field behaviour is via concentration tensors, which provide a measure of the deviation away from the mean fields throughout the material. Consider the identities

$$\langle \boldsymbol{\epsilon} \rangle_{\Omega} = \frac{1}{|\Omega|} \left(\int_{\Omega_1} \boldsymbol{\epsilon} \, d\Omega + \int_{\Omega_2} \boldsymbol{\epsilon} \, d\Omega \right) = v_1 \langle \boldsymbol{\epsilon} \rangle_{\Omega_1} + v_2 \langle \boldsymbol{\epsilon} \rangle_{\Omega_2}$$

and

$$\langle \boldsymbol{\sigma} \rangle_{\Omega} = \frac{1}{|\Omega|} \left(\int_{\Omega_1} \boldsymbol{\sigma} \, d\Omega + \int_{\Omega_2} \boldsymbol{\sigma} \, d\Omega \right) = v_1 \langle \boldsymbol{\sigma} \rangle_{\Omega_1} + v_2 \langle \boldsymbol{\sigma} \rangle_{\Omega_2}.$$

By direct manipulation we obtain

$$\begin{aligned} \langle \boldsymbol{\sigma} \rangle_{\Omega} &= v_1 \langle \boldsymbol{\sigma} \rangle_{\Omega_1} + v_2 \langle \boldsymbol{\sigma} \rangle_{\Omega_2} = v_1 \mathbb{E}_1 : \langle \boldsymbol{\epsilon} \rangle_{\Omega_1} + v_2 \mathbb{E}_2 : \langle \boldsymbol{\epsilon} \rangle_{\Omega_2} \\ &= \mathbb{E}_1 : (\langle \boldsymbol{\epsilon} \rangle_{\Omega} - v_2 \langle \boldsymbol{\epsilon} \rangle_{\Omega_2}) + v_2 \mathbb{E}_2 : \langle \boldsymbol{\epsilon} \rangle_{\Omega_2} \\ &= ((\mathbb{E}_1 + v_2(\mathbb{E}_2 - \mathbb{E}_1)) : \mathbf{C}) : \langle \boldsymbol{\epsilon} \rangle_{\Omega}, \end{aligned} \quad (5.3)$$

where

$$\underbrace{\left(\frac{1}{v_2} (\mathbb{E}_2 - \mathbb{E}_1)^{-1} : (\mathbb{E}^* - \mathbb{E}_1) \right)}_{\stackrel{\text{def}}{=} \mathbf{C}} : \langle \boldsymbol{\epsilon} \rangle_{\Omega} = \langle \boldsymbol{\epsilon} \rangle_{\Omega_2}. \quad (5.4)$$

Thereafter, we may write, for the variation in the stress

$$\mathbf{C} : \mathbb{E}^{*-1} : \langle \boldsymbol{\sigma} \rangle_{\Omega} = \mathbb{E}_2^{-1} : \langle \boldsymbol{\sigma} \rangle_{\Omega_2},$$

which reduces to

$$\mathbb{E}_2 : \mathbf{C} : \mathbb{E}^{*-1} : \langle \boldsymbol{\sigma} \rangle_{\Omega} \stackrel{\text{def}}{=} \bar{\mathbf{C}} : \langle \boldsymbol{\sigma} \rangle_{\Omega} = \langle \boldsymbol{\sigma} \rangle_{\Omega_2}. \quad (5.5)$$

$\bar{\mathbf{C}}$ is known as the stress concentration tensor. Therefore, once either $\bar{\mathbf{C}}$ or \mathbb{E}^* is known, the other can be determined. In the case of isotropy we may write

$$\bar{C}_{\kappa} \stackrel{\text{def}}{=} \frac{1}{v_2} \frac{\kappa_2 \kappa^* - \kappa_1}{\kappa^* \kappa_2 - \kappa_1} \quad \text{and} \quad \bar{C}_{\mu} \stackrel{\text{def}}{=} \frac{1}{v_2} \frac{\mu_2 \mu^* - \mu_1}{\mu^* \mu_2 - \mu_1}, \quad (5.6)$$

where $\bar{C}_{\kappa} \langle \frac{1}{3} \text{tr} \boldsymbol{\sigma} \rangle_{\Omega} = \frac{1}{3} \langle \text{tr} \boldsymbol{\sigma} \rangle_{\Omega_2}$ and $\bar{C}_{\mu} \langle \boldsymbol{\sigma}' \rangle_{\Omega} = \langle \boldsymbol{\sigma}' \rangle_{\Omega_2}$. Clearly, the microstress fields are minimally distorted when $\bar{C}_{\kappa} = \bar{C}_{\mu} = 1$. For the matrix, since

$$\langle \boldsymbol{\sigma} \rangle_{\Omega_1} = \frac{\langle \boldsymbol{\sigma} \rangle_{\Omega} - v_2 \langle \boldsymbol{\sigma} \rangle_{\Omega_2}}{v_1},$$

therefore

$$\langle \boldsymbol{\sigma} \rangle_{\Omega_1} = \frac{\langle \boldsymbol{\sigma} \rangle_{\Omega} - v_2 \bar{\mathbf{C}} : \langle \boldsymbol{\sigma} \rangle_{\Omega}}{v_1} = \frac{(1 - v_2 \bar{\mathbf{C}}) : \langle \boldsymbol{\sigma} \rangle_{\Omega}}{v_1} = \bar{\bar{\mathbf{C}}} : \langle \boldsymbol{\sigma} \rangle_{\Omega}, \quad (5.7)$$

and therefore, in the case of isotropy,

$$\bar{\bar{C}}_{\kappa} \stackrel{\text{def}}{=} \frac{1}{v_1} (1 - v_2 \bar{C}_{\kappa}) \quad \text{and} \quad \bar{\bar{C}}_{\mu} \stackrel{\text{def}}{=} \frac{1}{v_1} (1 - v_2 \bar{C}_{\mu}). \quad (5.8)$$

Therefore, for the deviation in the particulate stress fields away from the mean

$$\left| \frac{\langle \text{tr} \boldsymbol{\sigma} \rangle_{\Omega_2} - \text{tr} \boldsymbol{\sigma} \rangle_{\Omega}}{\langle \text{tr} \boldsymbol{\sigma} \rangle_{\Omega_2}} \right| = \left| \frac{\bar{C}_{\kappa} - 1}{\bar{C}_{\kappa}} \right| \quad (5.9)$$

and

$$\sqrt{\frac{(\langle \boldsymbol{\sigma}' \rangle_{\Omega_2} - \langle \boldsymbol{\sigma}' \rangle_{\Omega}) : (\langle \boldsymbol{\sigma}' \rangle_{\Omega_2} - \langle \boldsymbol{\sigma}' \rangle_{\Omega})}{\langle \boldsymbol{\sigma}' \rangle_{\Omega_2} : \langle \boldsymbol{\sigma}' \rangle_{\Omega_2}}} = \left| \frac{\bar{C}_{\mu} - 1}{\bar{C}_{\mu}} \right|, \quad (5.10)$$

and for the matrix material

$$\left| \frac{\langle \text{tr} \boldsymbol{\sigma} \rangle_{\Omega_1} - \langle \text{tr} \boldsymbol{\sigma} \rangle_{\Omega}}{\langle \text{tr} \boldsymbol{\sigma} \rangle_{\Omega_1}} \right| = \left| \frac{\bar{\bar{C}}_{\kappa} - 1}{\bar{\bar{C}}_{\kappa}} \right| \quad (5.11)$$

and

$$\sqrt{\frac{(\langle \boldsymbol{\sigma}' \rangle_{\Omega_1} - \langle \boldsymbol{\sigma}' \rangle_{\Omega}) : (\langle \boldsymbol{\sigma}' \rangle_{\Omega_1} - \langle \boldsymbol{\sigma}' \rangle_{\Omega})}{\langle \boldsymbol{\sigma}' \rangle_{\Omega_1} : \langle \boldsymbol{\sigma}' \rangle_{\Omega_1}}} = \left| \frac{\bar{\bar{C}}_{\mu} - 1}{\bar{\bar{C}}_{\mu}} \right|. \quad (5.12)$$

In order to incorporate the deviation in a cost function we introduce a tolerance, where, ideally,

$$\left| \frac{\bar{C}_\kappa - 1}{\bar{C}_\kappa} \right| \leq \text{tol}_\kappa \quad \text{and} \quad \left| \frac{\bar{C}_\mu - 1}{\bar{C}_\mu} \right| \leq \text{tol}_\mu \quad (5.13)$$

and

$$\left| \frac{\bar{\bar{C}}_\kappa - 1}{\bar{\bar{C}}_\kappa} \right| \leq \text{tol}_\kappa \quad \text{and} \quad \left| \frac{\bar{\bar{C}}_\mu - 1}{\bar{\bar{C}}_\mu} \right| \leq \text{tol}_\mu. \quad (5.14)$$

If the normalized deviation exceeds the corresponding tol, then the level of exceedance is incorporated as a multilateral constraint to the macroscopic objectives. As an example, our immediate goal is to design computationally the macroscale effective bulk and shear moduli κ^* and μ^* by using convex combinations of the Hashin–Shtrikman bounds as approximations for the effective moduli $\kappa^* \approx \theta\kappa^{*+} + (1-\theta)\kappa^{*-}$ and $\mu^* \approx \theta\mu^{*+} + (1-\theta)\mu^{*-}$, where $0 \leq \theta \leq 1$. The micro-macro-objective function is

$$\begin{aligned} \Pi = & w_1 \left| \frac{\kappa^*}{\kappa^{*,D}} - 1 \right|^p + w_2 \left| \frac{\mu^*}{\mu^{*,D}} - 1 \right|^p + \hat{w}_3 \left(\left| \frac{((\bar{C}_\kappa - 1)/\bar{C}_\kappa)}{\text{tol}_\kappa} \right| - 1 \right)^q \\ & + \hat{w}_4 \left(\left| \frac{((\bar{C}_\mu - 1)/\bar{C}_\mu)}{\text{tol}_\mu} \right| - 1 \right)^q + \hat{w}_5 \left(\left| \frac{((\bar{\bar{C}}_\kappa - 1)/\bar{\bar{C}}_\kappa)}{\text{tol}_\kappa} \right| - 1 \right)^q \\ & + \hat{w}_6 \left(\left| \frac{((\bar{\bar{C}}_\mu - 1)/\bar{\bar{C}}_\mu)}{\text{tol}_\mu} \right| - 1 \right)^q, \end{aligned} \quad (5.15)$$

where

- (i) if $|(\bar{C}_\kappa - 1)/\bar{C}_\kappa| \leq \text{tol}_\kappa$, then $\hat{w}_3 = 0$,
- (ii) if $|(\bar{C}_\kappa - 1)/\bar{C}_\kappa| > \text{tol}_\kappa$, then $\hat{w}_3 = w_3$,
- (iii) if $|(\bar{C}_\mu - 1)/\bar{C}_\mu| \leq \text{tol}_\mu$, then $\hat{w}_4 = 0$,
- (iv) if $|(\bar{C}_\mu - 1)/\bar{C}_\mu| > \text{tol}_\mu$, then $\hat{w}_4 = w_4$,
- (v) if $|(\bar{\bar{C}}_\kappa - 1)/\bar{\bar{C}}_\kappa| \leq \text{tol}_\kappa$, then $\hat{w}_5 = 0$,
- (vi) if $|(\bar{\bar{C}}_\kappa - 1)/\bar{\bar{C}}_\kappa| > \text{tol}_\kappa$, then $\hat{w}_5 = w_5$,
- (vii) if $|(\bar{\bar{C}}_\mu - 1)/\bar{\bar{C}}_\mu| \leq \text{tol}_\mu$, then $\hat{w}_6 = 0$,
- (viii) if $|(\bar{\bar{C}}_\mu - 1)/\bar{\bar{C}}_\mu - 1| > \text{tol}_\mu$, then $\hat{w}_6 = w_6$.

Here the design variables are $\mathbf{A} = \{\kappa_2, \mu_2 v_2\}$, and their constrained ranges are

$$\kappa_2^{(-)} \leq \kappa_2 \leq \kappa_2^{(+)}, \quad \mu_2^{(-)} \leq \mu_2 \leq \mu_2^{(+)}, \quad v_2^{(-)} \leq v_2 \leq v_2^{(+)}. \quad (5.16)$$

There are two characteristics of such a formulation which make the application of standard gradient-type minimization schemes, such as Newton's method, inapplicable. Firstly, the incorporation of limits on the microfield behaviour, as well as design

search space restrictions, renders the objective function not continuously differentiable in design space, and secondly, the objective function is non-convex, i.e. the system Hessian is not positive definite (invertible) throughout design space.

We consider a base matrix material (aluminium) of fixed material values,

$$\kappa_1 = 77.9 \text{ GPa} \quad \text{and} \quad \mu_1 = 25.9 \text{ GPa}.$$

The desired values are

$$\kappa^{*,D} = 96 \text{ GPa}, \quad \mu^{*,D} = 42 \text{ GPa}, \quad \text{tol}_\kappa = 0.5, \quad \text{tol}_\mu = 0.5.$$

The (constrained) design variable's ranges are

$$\begin{aligned} 0.1\kappa_1 &= \kappa_2^{(-)} \leq \kappa_2 \leq \kappa_2^{(+)} = 10\kappa_1, \\ 0.1\mu_1 &= \mu_2^{(-)} \leq \mu_2 \leq \mu_2^{(+)} = 10\mu_1, \\ 0 &= v_2^{(-)} \leq v_2 \leq v_2^{(+)} = \frac{2}{3}. \end{aligned}$$

The weights were set to $w_1 = w_2 = \hat{w}_3 = \hat{w}_4 = \hat{w}_5 = \hat{w}_6 = 1$. We used $\theta = 0.5$ for the Hashin–Shtrikman bound combination. The number of genetic strings was set to 1000, for 10 generations, keeping the offspring of the top 100 parents after each generation. Two cases were considered: (i) additionally keeping the top $K = 100$ parents after each generation, thus with 800 new genetic strings infused and (ii) not keeping the top $K = 100$ parents after each generation, thus with 900 new genetic strings infused. Figure 4 depicts the results for several generations. After 10 generations, a dominant genetic has appeared for each approach ((i) and (ii)). The minimization of the cost function is guaranteed to be monotone if the top parents are retained, i.e. $\Pi(\mathbf{A}^{\text{opt},I}) \geq \Pi(\mathbf{A}^{\text{opt},I+1})$, where $\mathbf{A}^{\text{opt},I+1}$ and $\mathbf{A}^{\text{opt},I}$ are the best genetic strings from generations $I + 1$ and I , respectively. There is no such guarantee if the top parents are not retained. While the non-retention of parents allows more newer genetic strings to be evaluated in the next generation, numerical studies conducted thus far imply, for sufficiently large populations, that the benefits of parent retention outweigh this advantage, as well as any disadvantages of ‘inbreeding’, i.e. a stagnant population. The case of inbreeding is circumvented in the current algorithm due to the fact that, with each new generation, new material designs, selected at random within the design space, are introduced into the population. As the results illustrate (table 1), not retaining the parents is suboptimal due to the possibility that inferior offspring will replace superior parents. Furthermore, parent retention is computationally less expensive, since these designs do not have to be re-evaluated, although this was not a concern for the types of simulations in this semi-analytical example.

6. Direct computational approaches

In order to perform meaningful computational optimization of the material microstructure, one needs reliable effective responses. It is clear that for the relation between averages to be useful, i.e. statistically representative, the sample must be so large that, for further enlargements, \mathbb{E}^* changes minimally. For illustration purposes, we used an aluminium (matrix)/boron (particle) combination. Typically, the boron ($\kappa_2 = 230 \text{ GPa}$, $\mu_2 = 172 \text{ GPa}$) is used as a stiffener for the aluminium matrix

Table 1. *Top designs after 10 generations*

(KPC, keeping parents with constraints; NKPC, not keeping parents with constraints; KPNC, keeping parents with no constraints; NKPNC, not keeping parents with no constraints.)

| search | $\frac{\kappa_2}{\kappa_1}$ | $\frac{\mu_2}{\mu_1}$ | v_2 | Π |
|--------|-----------------------------|-----------------------|---------|-----------------|
| KPC | 1.972 | 4.755 | 0.3179 | 0.000 000 009 8 |
| NKPC | 2.172 | 5.730 | 0.277 1 | 0.000 000 487 4 |
| KPNC | 2.377 | 6.753 | 0.246 6 | 0.000 000 005 7 |
| NKPNC | 2.507 | 7.408 | 0.231 1 | 0.000 005 661 0 |

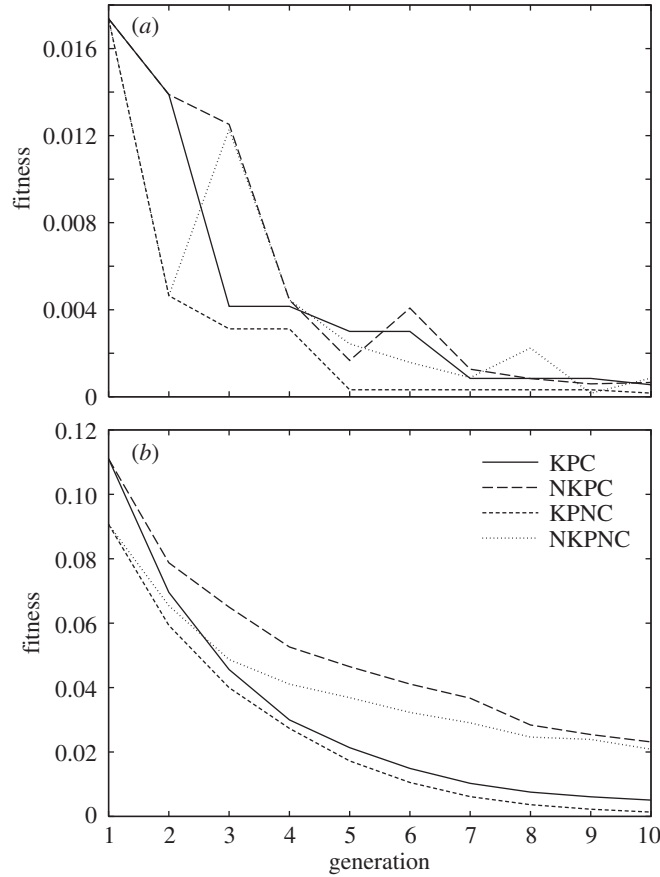


Figure 4. Generational values of (a) the best design's objective function and (b) the average of the best 10 designs' objective functions. KPC, keeping parents with constraints; NKPC, not keeping parents with constraints; KPNC, keeping parents with no constraints; NKPNC, not keeping parents with no constraints.

($\kappa_1 = 77.9$ GPa, $\mu_1 = 25.9$ GPa). We used a moderate particulate volume fraction of *ca.* 22%. The following particle-per-sample sequence (figure 5) was used to study the dependence of the effective responses on the sample size: 2 (5184 DOF), 4 (10 125 DOF), 8 (20 577 DOF), 16 (41 720 DOF), 32 (81 000 DOF) and 64 (151 959

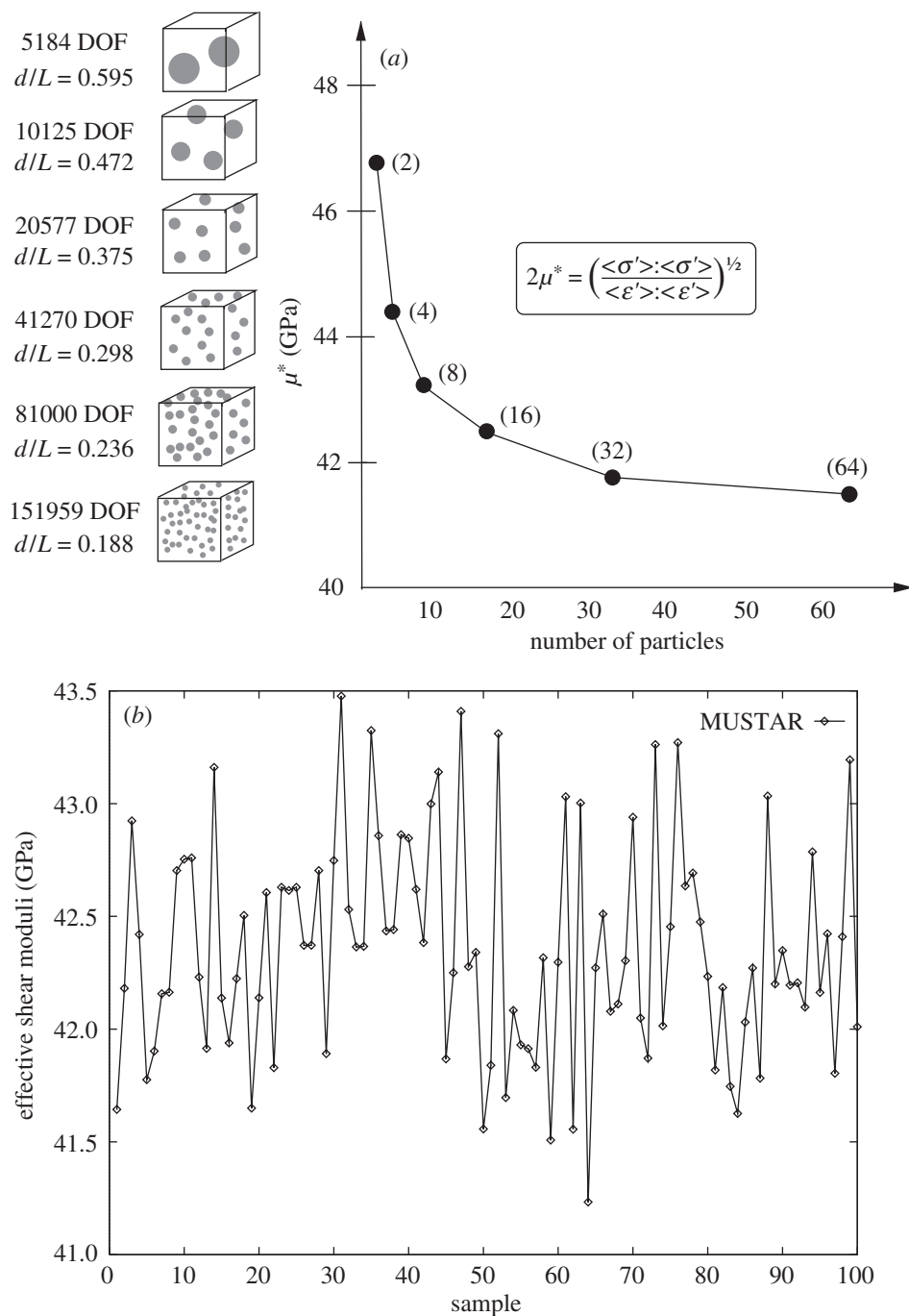


Figure 5. (a) The values of the effective shear responses for samples containing increasingly larger numbers of particles. One hundred tests were performed per particle/sample combination and the results were averaged. (b) 100 samples: shear responses, μ^* , of a block with 20 randomly distributed boron spheres embedded in an aluminium matrix. Each point represents the results of one test.

DOF) particles, where ‘DOF’ denotes the degrees of freedom. For more details on the finite-element implementation, we refer the reader to the appendix. A meaningful parameter to track was the ratio of the diameter of the individual particles (d) to the length of the sample (L). Throughout the tests, we considered a single combined boundary loading satisfying Hill’s condition, $\mathbf{u}|_{\partial\Omega} = \mathcal{E} \cdot \mathbf{x}$, $\mathcal{E}_{ij} = 0.001$, $i, j = 1, 2, 3$. We tracked the effective bulk and shear moduli, κ^* and μ^* , respectively. At each sample size, size effects, i.e. scatter in the effective responses, occur. To eliminate the effects of scatter, the tests were performed 100 times for each sample size (each time with a different random-particulate distribution) and the responses averaged.† Since the effective bulk and shear responses behave in a quantitatively similar manner, for brevity, we show only the effective shear responses. Figure 5 depicts the dependency of the responses with growth in particle number per sample, keeping the volume fraction constant. For example, the time to preprocess, solve and postprocess a 20-particle sample finite-element test is roughly 10 s on a single workstation, using a research code written by the author.‡ For three successive enlargements of the number of particles, i.e. 16-, 32- and 64-particle samples, the responses differed from one another, on average, by less than 1%. One approach is to select reasonably large samples (for a given \mathbf{A}) with a fixed number of particles, for example 20. However, the samples will exhibit mutual fluctuations in their respective effective responses due to the various random-particulate realizations. A stabilization procedure is then applied, by which a series of the samples are tested until the progressive ensemble average converges. For example, consider a certain microstructural design specification (\mathbf{A}), and a process where a sample of finite size, with a random microstructure, is tested, and the effective response recorded. Consider a repetition of the test for another equally sized sample, with the same microstructural design vector but with another random microstructural realization. The tests are repeated, for more and more samples, until the sequential change in the ensemble average falls below a given tolerance for further tests ($i = 1, 2, \dots, S$):

$$\left| \frac{1}{S+1} \sum_{i=1}^{S+1} \Pi^{(i)} - \frac{1}{S} \sum_{i=1}^S \Pi^{(i)} \right| \leq \text{tol} \left| \frac{1}{S+1} \sum_{i=1}^{S+1} \Pi^{(i)} \right|. \quad (6.1)$$

Therefore, in step 2 of the algorithm in §5, one must only replace ‘compute’ with ‘ensemble-compute’. This procedure is quite effective in eliminating detrimental size-effect noise. For further theoretical analysis of size-effect perturbations see Huet (1982, 1984, 1990), Hazanov & Huet (1994), Hazanov & Amieur (1995) and Huet (1997, 1999). In particular, for the consequences of size effects on optima see Zohdi (2002c).

7. Numerical examples and closing remarks

A fixed mesh of *ca.* $9 \times 9 \times 9$ trilinear hexahedra or 2344 numerical degrees of freedom *per particle*, for a total 46 875 degrees of freedom, was used. This mesh density delivered mesh independent results over the course of the numerical experiments. In other

† This procedure can be done trivially in parallel.

‡ Of course, these tests could have been performed trivially in parallel, and thus the entire 100-sample testing run would have taken 10 s.

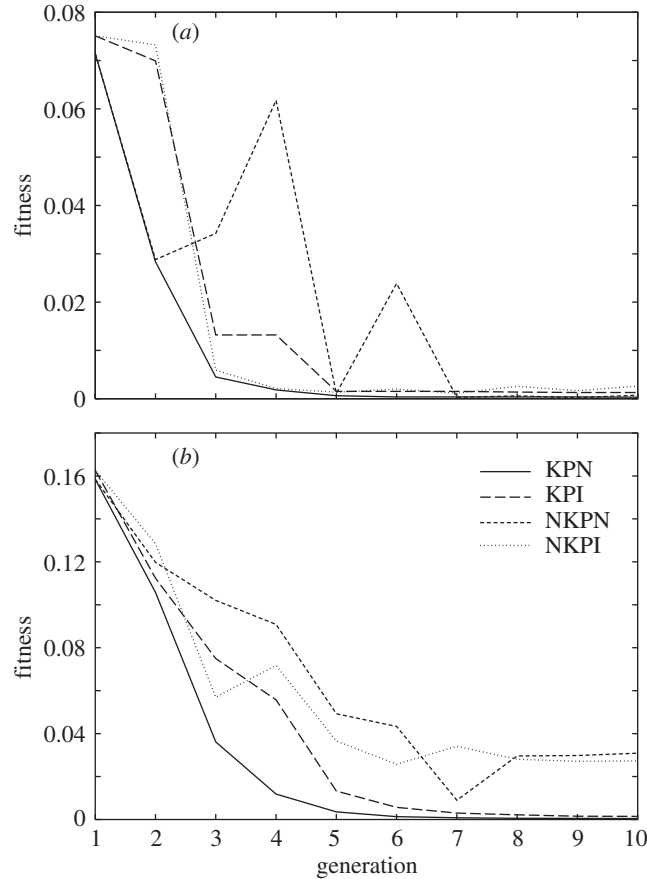


Figure 6. (a) Top design and (b) top six average designs after 10 generations. KPN, keep parents/non-isotropic; KPI, keep parents/isotropic; NKPN, not keep parents/non-isotropic; NKPI, not keep parents/isotropic.

words, the same final designs occurred using finer meshes. To illustrate the search process, continuing with 20-particle subsamples, the effective response produced by a sample containing *ca.* 22% boron spheres in an aluminium matrix ($\mu_1 = 25.9$ GPa, $\kappa_1 = 77.9$ GPa) was first computed. The effective response was *ca.* $\kappa^* = 96$ GPa and $\mu^* = 42$ GPa. Our objective was to find alternative microstructures which could deliver the same effective response ($\kappa^{*,D} = 96$ GPa and $\mu^{*,D} = 42$ GPa), while obeying the stress perturbation constraints, to a specified tolerance.† We considered an objective function of the following form:

$$\Pi = w_\kappa \underbrace{\left| \frac{\kappa^* - \kappa^{*,D}}{\kappa^{*,D}} \right|^p}_{\text{macroscopic bulk}} + w_\mu \underbrace{\left| \frac{\mu^* - \mu^{*,D}}{\mu^{*,D}} \right|^p}_{\text{macroscopic shear}} + w_\sigma \underbrace{\left(\frac{\sqrt{\langle \delta \boldsymbol{\sigma} : \delta \boldsymbol{\sigma} \rangle_\Omega} / \langle \boldsymbol{\sigma} : \boldsymbol{\sigma} \rangle_\Omega}{\text{tol}_\sigma} - 1 \right)^q}_{\text{microfield smoothness}}. \quad (7.1)$$

† Throughout the tests, we considered a single combined boundary loading satisfying Hill's condition, $\mathbf{u}|_{\partial\Omega} = \boldsymbol{\varepsilon} \cdot \mathbf{x}$, $\boldsymbol{\varepsilon}_{ij} = 0.001$, $i, j = 1, 2, 3$.

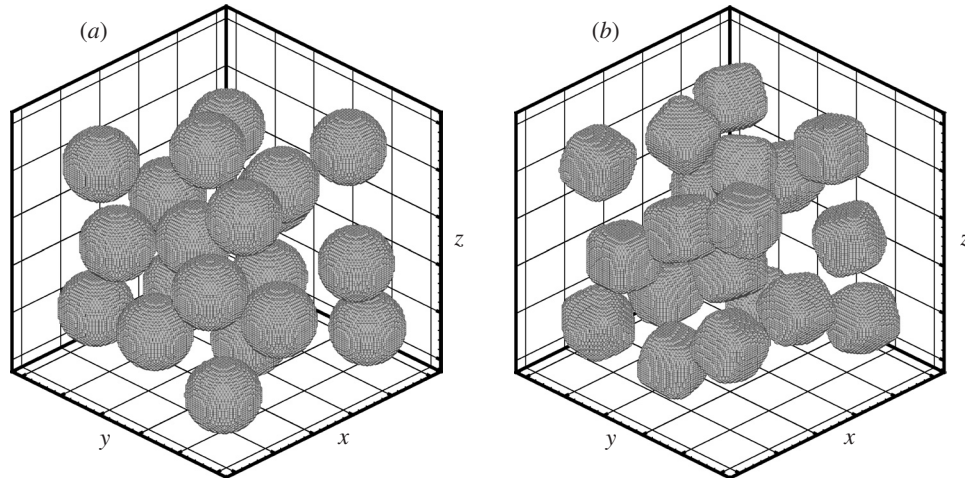


Figure 7. (a) The original spherical microstructure: $\kappa_2/\kappa_1 = 2.95$, $\mu_2/\mu_1 = 6.90$, $\zeta = 0.75$ (volume fraction: $v_2 \approx 0.22$), $A = 1$, $s = 2$. (b) A general alternative microstructure (to spheres) produced by minimizing the perturbation in the stresses within the material while maintaining the same effective response.

Table 2. *Top designs and average of the top six, after 10 generations*

(KP, keeping parents and with a non-isotropic polynomial order; KPIP, not keeping parents and with a non-isotropic polynomial order; NKP, keeping parents and with an isotropic polynomial order; NKPIP, not keeping parents and with an isotropic polynomial order.)

| search type | $\frac{\kappa_2}{\kappa_1}$ | $\frac{\mu_2}{\mu_1}$ | ζ | v_2 | A | s_1 | s_2 | s_3 | Π |
|-------------|-----------------------------|-----------------------|---------|-------|-------|-------|-------|-------|----------|
| KP | 5.540 | 6.349 | 0.358 | 0.183 | 1.373 | 5.155 | 7.055 | 7.901 | 0.000 32 |
| KPIP | 4.728 | 4.759 | 0.341 | 0.213 | 1.178 | 6.210 | 6.210 | 6.210 | 0.001 30 |
| NKP | 3.720 | 7.670 | 0.385 | 0.206 | 1.379 | 3.528 | 5.653 | 4.606 | 0.000 73 |
| NKPIP | 3.730 | 5.144 | 0.344 | 0.205 | 1.208 | 5.950 | 5.950 | 5.950 | 0.002 63 |

With this in mind, the algorithm was started away from the original spherical aluminium/boron design location, but still prescribing the same objective:

$$\kappa^{*,D} = 96 \text{ GPa} \quad \text{and} \quad \mu^{*,D} = 42 \text{ GPa}.$$

The matrix material was fixed to be aluminium, however, all other design parameters, with the exception of the particle orientations (since isotropic objectives were sought), were allowed to vary. We used the weights $w_\kappa = w_\mu = w_\sigma = 1$. The exponents $p = q = 1$ were used in equation (7.1). The constraints on the design space were

$$\begin{aligned} 0.1\kappa_1 &= \kappa_2^{(-)} \leq \kappa_2^i \leq \kappa_2^{(+)} = 10\kappa_1, \\ 0.1\mu_1 &= \mu_2^{(-)} \leq \mu_2^i \leq \mu_2^{(+)} = 10\mu_1, \\ 0.1 &= A^{(-)} \leq A^i \leq A^{(+)} = 10, \end{aligned}$$

$$1 = s^{(-)} \leq s^i \leq s^{(+)} = 10,$$

$$0.2 = \zeta^{(-)} \leq \zeta^i \leq \zeta^{(+)} = 0.4.$$

The volume fraction was controlled via a particle/sample size ratio (one variable), defined by a subvolume size $V \stackrel{\text{def}}{=} (L \times L \times L)/N$, where N is the number of particles in the entire sample and where L is the length of the (cubical) sample, $L \times L \times L$. A generalized diameter is defined, r , which is the diameter of the smallest sphere that can enclose a single particle of possibly non-spherical shape. The ratio between the generalized diameter and the subvolume is one design parameter defined by $\zeta \stackrel{\text{def}}{=} r/V^{1/3}$. The number of genetic strings was set to 20, for 10 generations keeping the offspring of the top six parents. Two cases were considered: keeping the top $K = 6$ parents and not keeping the top $K = 6$ parents and also keeping the polynomial order the same for all three axes and allowing all axes to vary. It appears that even for isotropic overall responses, allowing the polynomial order of the axes to vary appears to minimize the objective even further. Table 2 and figure 6 depict the results. As mentioned earlier, retaining the parents generates a better set of designs at the end of the multiple generation cycle. The total number of global evaluations is $T + (G - 1) \times (T - Q)$, where G is the number of generations, T is the total number of genetic strings in the population and Q is the number of parents kept after each generation. The minimization of the cost function is guaranteed to be monotonic, if the top parents are retained. For the best design, generated when retaining the parents and with non-isotropic topological exponents, 146 genetic strings were tested after 10 generations. A total of 1664 samples (each containing 20 particles) were tested to stabilize the ensemble averaging process, for an average of 11.8 with samples per string. The cuboid type microstructures that occur are similar to microstructures generated by Vigdergauz (1994, 2001*a, b*) and by Torquato & Hyun (2001), although they are for somewhat different objective functions in two dimensions for periodic media. Clearly, the rounding of the corners of the particles of the cuboid microstructure (figure 7) is a product of the stress-field constraints.

8. Concluding comments

The focus of the work presented here was the development of a statistical genetic algorithm which can handle difficulties due to objective function non-convexity, lack of regularity and size effects encountered in the design of random-particulate media. The computational approach was constructed so that it can be easily implemented by a wide audience of researchers in the field. Theoretical properties of the overall approach were investigated and semi-analytical and large-scale numerical examples, involving finite-element-type discretizations, were given to illustrate its practical application. Clearly, the approach presented is only one possible strategy to contend with the difficulties that one encounters in the design of random-particulate media. However, it is relatively straightforward to implement and does not require a significant coding effort.

Appendix A.

Throughout the simulations, we shall employ the finite-element method, along with a technique of Gauss-point oversampling to resolve the topological features of

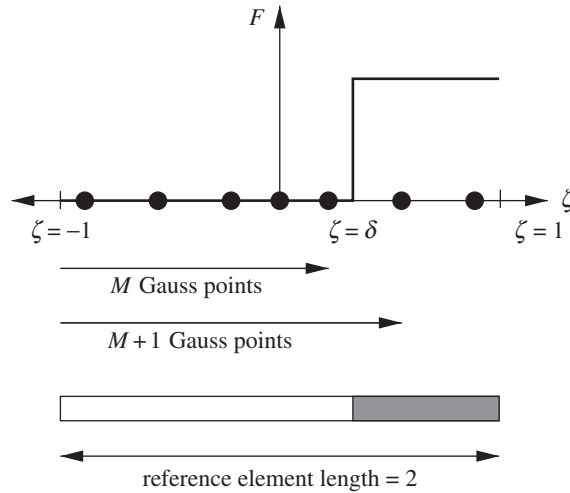
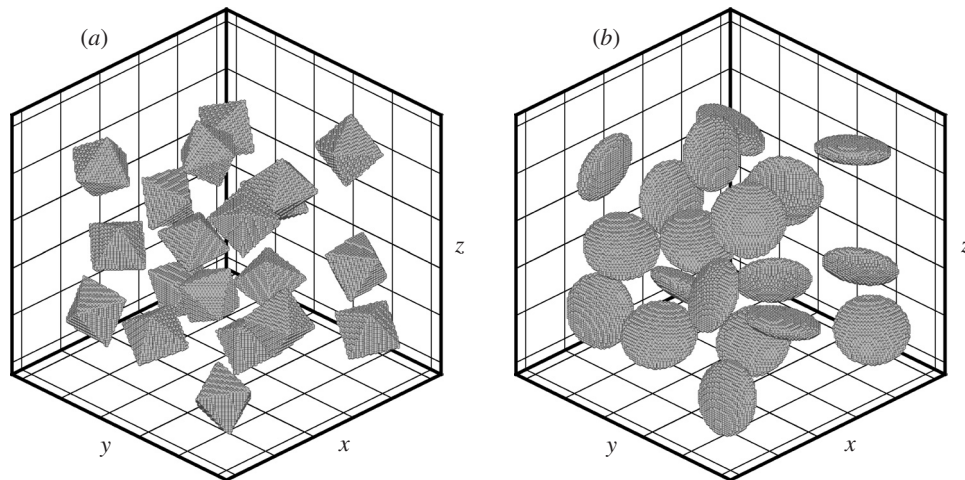


Figure 8. A material discontinuity in a reference finite element.

Figure 9. A random microstructure consisting of 20 non-intersecting particles. (a) Diamond-type microstructure ($s_1 = s_2 = s_3 = 1$). (b) Oblate disc-type microstructure (aspect ratio of 1 : 3). Both microstructures contain particles which occupy *ca.* 7% of the volume.

the microstructure accurately. We first consider a one-dimensional reference finite-element domain, and associated integrands, $F(\zeta)$ with a jump discontinuity at δ (figure 8), which admit a decomposition of the function into continuous and discontinuous parts, $F(\zeta) = C(\zeta) + \llbracket F(\delta) \rrbracket H(\zeta - \delta)$, where ζ is the local coordinate, and $\llbracket (\cdot) \rrbracket \stackrel{\text{def}}{=} (\cdot)|_+ - (\cdot)|_-$ is the jump operator. We assume that the elements are small compared with the length-scales of the particulate matter and as a consequence that there is at most one discontinuity within the element. However, this assumption makes no difference at the implementation level. Integrating over a reference element, we have $\int_{-1}^1 F(\zeta) d\zeta = \int_{-1}^1 (C(\zeta) + \llbracket F(\delta) \rrbracket H(\zeta - \delta)) d\zeta$. We perform a straightforward Gauss–Legendre quadrature, with G quadrature points, where m points lie before the discontinuity at δ . We assume that the continuous function,

possibly a polynomial, can be integrated exactly, or nearly exactly, with standard quadrature

$$\int_{-1}^1 C(\zeta) \, d\zeta \approx \sum_{i=1}^G C(\zeta_i) w_i,$$

where w_i are the Gauss weights and where ζ_i are the Gauss-point locations. We note the property $\sum_{i=1}^G w_i = 2$. The remainder is the discontinuous part,

$$\|F(\delta)\| \int_{-1}^1 H(\zeta - \delta) \, d\zeta = \|F(\delta)\| (1 - \delta).$$

We may write

$$\|F(\delta)\| \sum_{i=1}^G H(\zeta_i - \delta) w_i = \|F(\delta)\| \sum_{i=1}^m 0 \times w_i + \|F(\delta)\| \sum_{i=m+1}^G 1 \times w_i.$$

As a consequence, the maximum amount of variation in the computed integration is

$$\text{variation} = \|F(\delta)\| \left(\sum_{i=m}^G w_i - \sum_{i=m+1}^G w_i \right) \leq \|F(\delta)\| \max_i w_i. \quad (\text{A } 1)$$

In order to bound the dependence of the largest quadrature weight, w_i in the interval $(-1, 1)$, with the Gauss–Legendre rule, we fit the least-squares curves (Gauss rules of $1 \leq G \leq 10$) with $\max_{i \leq G} w_i \approx 1.93G^{-0.795}$ with $R^2 = 0.99$, where $R^2 = 1.0$ indicates a perfect regression value of the curve fit. Simple three-dimensional estimates can be made by applying this procedure in all three directions on a reference element.

For example, consider a three-dimensional step function discontinuity over a reference finite element $((-1, 1) \times (-1, 1) \times (-1, 1))$. Denoting the reference-element volumetric normalization of the bound by $\beta \stackrel{\text{def}}{=} \frac{1}{8} (1.93G^{-0.795})^3$, since $8 = 2 \times 2 \times 2$ is the volume of the reference element, one has for (i) a $2 \times 2 \times 2$ Gauss rule $\beta = 0.1720$, (ii) a $3 \times 3 \times 3$ Gauss rule $\beta = 0.0654$, (iii) a $4 \times 4 \times 4$ Gauss rule $\beta = 0.0329$ and (iv) a $5 \times 5 \times 5$ Gauss rule $\beta = 0.0193$. Consequently, the amount of variation in the integral is at most *ca.* 2%. Therefore, for efficient implementation, a 2/5 rule should be used, whereby a $2 \times 2 \times 2$ Gauss rule is used if there is no material discontinuity in the element, and a $5 \times 5 \times 5$ rule is used if there is a material discontinuity. We emphasize that this procedure is used simply to integrate elemental quantities with discontinuities accurately. For a variety of numerical tests in Zohdi (2001), the typical mesh density to deliver mesh insensitive results, for the quantities of interest in the upcoming simulations, was $9 \times 9 \times 9$ trilinear finite-element hexahedra (*ca.* 2200–3000 DOF) *per particle*. A disc-type and a diamond-type microstructure, as seen by the meshing algorithm with a $24 \times 24 \times 24$ trilinear hexahedra mesh density for a total of 46 875 DOF (*ca.* $9 \times 9 \times 9$ hexahedra or 2344 DOF per element), are shown in figure 9.

References

- Cherkaev, A. 2000 *Variational methods for structural optimization*. Springer.
 Davis, L. 1991 *Handbook of genetic algorithms*. London: International Thompson Computer Press.

- Gill, P., Murray, W. & Wright, M. 1995 *Practical optimization*. Academic.
- Goldberg, D. E. 1989 *Genetic algorithms in search, optimization and machine learning*. Addison-Wesley.
- Goldberg, D. E. & Deb, K. 2000 Special issue on genetic algorithms. *Comput. Meth. Appl. Mech. Engng* **186**, 121–124.
- Hashin, Z. & Shtrikman, S. 1962 On some variational principles in anisotropic and non-homogeneous elasticity. *J. Mech. Phys. Solids* **10**, 335–342.
- Hashin, Z. & Shtrikman, S. 1963 A variational approach to the theory of the elastic behaviour of multiphase materials. *J. Mech. Phys. Solids* **11**, 127–140.
- Hazanov, S. & Amieur, M. 1995 On overall properties of elastic heterogeneous bodies smaller than the representative volume. *Int. J. Engng Sci.* **33**, 1289–1301.
- Hazanov, S. & Huet, C. 1994 Order relationships for boundary conditions effect in heterogeneous bodies smaller than the representative volume. *J. Mech. Phys. Solids* **42**, 1995–2011.
- Hill, R. 1952 The elastic behaviour of a crystalline aggregate. *Proc. Phys. Soc. Lond.* A **65**, 349–354.
- Holland, J. H. 1975 *Adaptation in natural and artificial systems*. Ann Arbor, MI: University of Michigan Press.
- Huet, C. 1982 Universal conditions for assimilation of a heterogeneous material to an effective medium. *Mech. Res. Commun.* **9**, 165–170.
- Huet, C. 1984 On the definition and experimental determination of effective constitutive equations for heterogeneous materials. *Mech. Res. Commun.* **11**, 195–200.
- Huet, C. 1990 Application of variational concepts to size effects in elastic heterogeneous bodies. *J. Mech. Phys. Solids* **38**, 813–841.
- Huet, C. 1997 An integrated micromechanics and statistical continuum thermodynamics approach for studying the fracture behaviour of microcracked heterogeneous materials with delayed response. *Engng Fract. Mech.* **58**, 459–556.
- Huet, C. 1999 Coupled size and boundary condition effects in viscoelastic heterogeneous bodies. *Mech. Mater.* **31**, 787–829.
- Hyun, S. & Torquato, S. 2001 Designing material microstructures with target properties. *J. Mater. Res.* **16**, 280.
- Michaud, V. 1992 Liquid state processing. In *Fundamentals of metal–matrix composites* (ed. S. Suresh, A. Mortensen & A. Needleman). Boston, MA: Butterworth-Heinemann.
- Onwubiko, C. 2000 *Introduction to engineering design optimization*. Englewood Cliffs, NJ: Prentice Hall.
- Torquato, S. 1991 Random heterogeneous media: microstructure and improved bounds on effective properties. *Appl. Mech. Rev.* **44**, 37–76.
- Torquato, S. 1997 Effective stiffness tensor of composite media. I. Exact series expansions. *J. Mech. Phys. Solids* **45**, 1421–1448.
- Torquato, S. 1998 Effective stiffness tensor of composite media. II. Applications to isotropic dispersions. *J. Mech. Phys. Solids* **46**, 1411–1440.
- Torquato, S. 2002 *Random heterogeneous materials: microstructure and macroscopic properties*. Springer.
- Torquato, S. & Hyun, S. 2001 Effective-medium approximation for composite media: realizable single-scale dispersions. *J. Appl. Phys.* **89**, 1725–1729.
- Vigdergauz, S. 1994 Three-dimensional grained composites of extreme thermal properties. *J. Mech. Phys. Solids* **42**, 729–740.
- Vigdergauz, S. 2001a Genetic algorithm perspective to identify energy optimizing inclusions in an elastic plate. *Int. J. Solids Struct.* **38**, 6851–6867.
- Vigdergauz, S. 2001b The effective properties of a perforated elastic plate: numerical optimization by genetic algorithm. *Int. J. Solids Struct.* **38**, 8593–8616.

- Zohdi, T. I. 2001 Computational optimization of vortex manufacturing of advanced materials. *Comput. Meth. Appl. Mech. Engng* **190**, 6231–6256.
- Zohdi, T. I. 2002a Incorporation of microfield distortion into rapid effective property design. *Math. Mech. Solids* **7**, 237–254.
- Zohdi, T. I. 2002b On the tailoring of microstructures for prescribed effective properties. *Int. J. Fract.* **114**, L15–L20.
- Zohdi, T. I. 2002c Bounding envelopes in multiphase material design. *J. Elastic.* **66**, 47–62.

